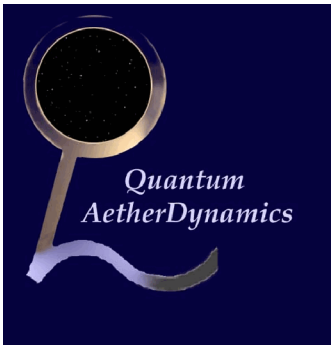

Quantum AetherDynamics Institute (QADI)

Field-Aligned Current Closure in APM/QMU: A Ledger-First Circuit Template Inspired by Alfvén

David W. Thomson III
Quantum AetherDynamics Institute (QADI), Alma, Illinois, USA
ORCID: 0000-0002-5830-5427

Version 1.0 – January 11, 2026

This article is published by the Quantum AetherDynamics Institute (QADI).

It develops the Aether Physics Model (APM)

Abstract

This template paper sets a ledger-first framework for magnetosphere–ionosphere coupling using Quantum Measurement Units (QMU) and the Aether Physics Model (APM), with an emphasis on field-aligned (Birkeland) current closure in the spirit of Alfvén's circuit viewpoint. We introduce a minimal set of dimensionless observables for field-aligned current, parallel potential drop, and an effective acceleration-channel resistance (normalized in resn units). These observables are constructed to remain internal to the APM ledger, using the Aether rotational identity (Ledger One) as the propagation anchor. We propose three falsifiable "gates" (A1–A3) that can be evaluated on spacecraft and ground-based datasets: resistance clustering, monotone closure under driving, and saturation as a ledger cap. No SI units are used; all statements are made in QMU-native form.

Contents

1 Introduction **3**

1.1 Problem statement . . . 3

1.2 Scope and exclusions . . . 3

2 Background: Alfvén Circuit View of FAC Closure **3**

2.1 Generator–transmission–load decomposition . . . 3

2.2 Why a ledger-first formulation is useful . . . 3

3 APM/QMU Normalization **4**

3.1 Ledger One as the propagation anchor . . . 4

3.2 Notation: QMU curl (unit) versus vector-calculus curl (operator) . . . 4

3.3 Charge convention and the resn unit (resistance) . . . 4

3.4 APM impedance/admittance analogs . . . 5

4 Dimensionless FAC Observables **5**

4.1 Starred length coordinate . . . 5

4.2 Dimensionless parallel electric field and potential drop . . . 5

4.3 Dimensionless current . . . 6

4.4 Effective acceleration-channel resistance (in resn units) . . . 6

4.5 Optional: dimensionless current density . . . 6

5 Ledger-First Closure Hypothesis for FAC Systems **6**

5.1 Closure postulate . . . 6

5.2 Interpretive map 6

6 Falsifiable Gates (A1–A3) 7

6.1 Gate A1: Resistance clustering 7

6.2 Gate A2: Monotone closure under driving 7

6.3 Gate A3: Saturation as a ledger cap 7

7 Data Products and Inference in Starred Variables 8

7.1 What must be inferred (minimal closure tuple) 8

7.2 FAC inference pathway (magnetometer-derived products) 8

7.3 Parallel potential drop inference pathway 9

7.4 Effective resistance and power in starred form 9

7.5 Geometry normalization (what must be recorded) 10

7.6 Practical note on “ledger proxies” 10

7.7 Toy numerical illustration (resn-normalized) and actionable gate checks 10

8 APM Predictions Beyond the Gates (Optional Extensions) 12

8.1 Channel “impedance” selection 12

8.2 Multi-channel closure 12

9 Proposed Experiments and Observation Campaigns 12

9.1 Archive-only retrospective test (no new hardware) 12

9.2 Targeted conjunction test 12

9.3 Laboratory analog (optional) 12

10 Discussion 12

10.1 Interpretation of outcomes 12

10.2 Relation to other APM work 13

11 Conclusion 13

A Algebraic identities from Ledger One 13

B Notes on sign/orientation conventions 13

1 Introduction

1.1 Problem statement

Field-aligned currents (FACs) are among the cleanest contexts in which to treat electromagnetic power flow as a global closure problem: a generator region drives, a transmission channel conveys, and a load region closes. The large-scale Region 1/Region 2 current systems established from low-altitude observations provide a canonical reference structure for this closure viewpoint [Iijima and Potemra, 1976, 1978, Coxon et al., 2018]. This paper provides a QMU/APM template for formalizing that viewpoint as a ledger closure statement with testable consequences.

1.2 Scope and exclusions

We focus on the circuit/closure structure and on dimensionless observables that can be inferred from standard data products. Detailed kinetic derivations (e.g., distribution functions, full two-fluid closures) are intentionally deferred to appendices or future papers.

2 Background: Alfvén Circuit View of FAC Closure

2.1 Generator–transmission–load decomposition

In Alfvén's circuit language, large-scale plasma electrodynamics is most transparently organized as a generator–transmission–load system, where currents and potential drops are not incidental but are the primary book-keeping objects of the dynamics [Alfvén, 1981]. For terrestrial auroral coupling, an operational decomposition is:

- **Generator:** solar-wind/magnetosphere driving and global reconnection-imposed boundary conditions.
- **Transmission:** Alfvénic coupling along flux tubes that carries stress and energy to the ionosphere.
- **Load:** ionospheric dissipation and localized acceleration structures (double layers, quasi-static parallel fields) that realize closure [Mozer and Hull, 2001, Carlson et al., 1998, Ergun et al., 2004].

2.2 Why a ledger-first formulation is useful

Many idealized magnetofluid treatments compress circuit closure into local constitutive relations; however, FAC systems routinely exhibit boundary-layer operators (e.g., double layers) that behave like discrete closure elements rather than smoothly varying resistors [Ergun et al., 2004, Knight, 1973, Morooka et al., 2004]. In APM/QMU, closure is taken as primary and expressed in ledger-native invariants; the observational question becomes whether inferred starred variables exhibit the discrete/structured behavior implied by ledger closure.

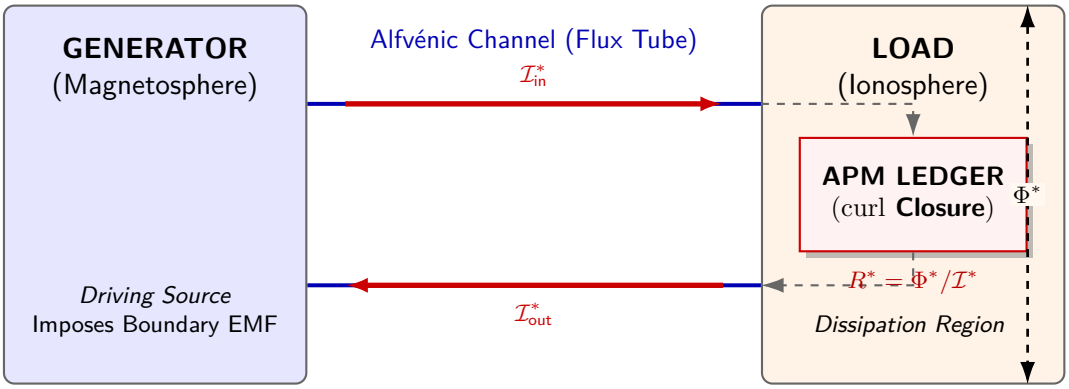

Figure 1: **APM Ledger-First Circuit Template.** By separating the layout components, this diagram clearly illustrates the flow: The Magnetosphere (left) drives the circuit, but the closure is determined by the APM Ledger (center red box), which mathematically enforces the resistance mode R^*.

3 APM/QMU Normalization

3.1 Ledger One as the propagation anchor

We adopt the standardized Ledger One closure statement:

$$A_u \cdot \text{curl} = {F_q}^2 {\lambda_C}^2. \tag{1}$$

With the mainstream bridge

$$c := F_q \lambda_C, \tag{2}$$

Ledger One is equivalently

$$A_u \cdot \text{curl} = c^2. \tag{3}$$

3.2 Notation: QMU curl (unit) versus vector-calculus curl (operator)

Throughout, curl denotes the *QMU torsional unit* defined in APM/QMU (a scalar ledger quantity with an optional orientation convention). It is *not* the vector-calculus operator $\nabla \times (\cdot)$. When the operator is needed, we write it explicitly as $\nabla \times (\cdot)$.

3.3 Charge convention and the resn unit (resistance)

Unless explicitly working in a plasma formulation where e^2 appears naturally, we take the QMU base charge to be

$$\text{chrg} \equiv {e_{\text{emax}}}^2,$$

and treat e^2 as a derived quantity related by

$$e^2 = 8\pi\alpha\, {e_{\text{emax}}}^2, \qquad {e_{\text{emax}}}^2 = \frac{e^2}{8\pi\alpha}. \tag{4}$$

This keeps circuit quantities ledger-native and makes the charge conversion factor explicit whenever plasma-derived expressions are imported.

For reference, the circuit-unit relations used in this template are

$$\text{potn} := \frac{\text{enrg}}{{e_{\text{emax}}}^2}, \qquad \text{curr} := {e_{\text{emax}}}^2\, F_q, \qquad \text{resn} := \frac{\text{mflx}}{{e_{\text{emax}}}^2}. \tag{5}$$

With the QMU composite

$$\text{mflx} := \frac{m_{\text{e}}\, {\lambda_C}^2 F_q}{{e_{\text{emax}}}^2},$$

the resistance unit becomes

$$\text{resn} = \frac{\text{mflx}}{{e_{emax}}^2} = \frac{m_{\text{e}}\, {\lambda_C}^2 F_q}{{e_{emax}}^4}, \tag{6}$$

so "resistance in resn units" is implemented simply by using ${e_{\text{emax}}}^2$ (not e^2) as the base charge in the starred observables below.

3.4 APM impedance/admittance analogs

Define ledger-native "line" parameters:

$$Z_{\text{APM}} := \sqrt{\frac{A_u}{\text{curl}}}, \qquad Y_{\text{APM}} := \sqrt{\frac{\text{curl}}{A_u}}. \tag{7}$$

Using Eq. (3), for positive magnitudes of curl one may write

$$Z_{\text{APM}} = \frac{c}{\text{curl}}, \qquad Y_{\text{APM}} = \frac{\text{curl}}{c}, \tag{8}$$

noting that if a signed orientation convention is used for curl, then $Z_{\text{APM}} = c/\left|\text{curl}\right|$ is the scalar magnitude.

4 Dimensionless FAC Observables

4.1 Starred length coordinate

Normalize field-aligned distance ℓ by λ_C:

$$\ell^* := \frac{\ell}{\lambda_C}, \qquad \mathrm{d}\ell = \lambda_C\, \mathrm{d}\ell^*. \tag{9}$$

4.2 Dimensionless parallel electric field and potential drop

Define a dimensionless parallel electric field by choosing a QMU-native force-per-charge scale:

$$\mathcal{E}_{\parallel}^* := \frac{E_{\parallel}}{m_{\text{e}}\, {F_q}^2 \lambda_C / {e_{\text{emax}}}^2}. \tag{10}$$

Then the dimensionless field-aligned potential drop is

$$\Phi^* := \int \mathcal{E}_{\parallel}^*\, \mathrm{d}\ell^*. \tag{11}$$

4.3 Dimensionless current

Define the dimensionless current as charge-throughput normalized by ${e_{\mathrm{emax}}}^2$ per quantum time:

$$\mathcal{I}^* := \frac{\dot{Q}}{{e_{\mathrm{emax}}}^2 F_q}. \tag{12}$$

This is the minimal FAC observable: it quantifies throughput without committing to a specific microscopic carrier model. (If a plasma formulation introduces e^2, apply Eq. (4) to return to the ${e_{\mathrm{emax}}}^2$ base.)

4.4 Effective acceleration-channel resistance (in resn units)

Define the effective (dimensionless) resistance of the acceleration region:

$$R^* := \frac{\Phi^*}{\mathcal{I}^*}. \tag{13}$$

By construction, R^* is the resistance expressed in resn units (cf. Eq. (6)): equivalently,

$$R_{\mathrm{APM}} = R^* \,\mathrm{resn}.$$

4.5 Optional: dimensionless current density

If a flux-tube cross-section area A is used, define the normalized current density:

$$\mathcal{J}_\parallel^* := \frac{J_\parallel}{{e_{\mathrm{emax}}}^2 F_q/{\lambda_C}^2}. \tag{14}$$

This requires a geometric model for mapping spacecraft crossings to a tube cross-section.

5 Ledger-First Closure Hypothesis for FAC Systems

5.1 Closure postulate

> For a given flux-tube geometry, the FAC system selects $(\mathcal{I}^*, \Phi^*)$ so that electromagnetic power transport closes in the APM ledger variables (A_u, curl) across generator, transmission, and load. When smooth closure fails, the system forms discrete boundary operators (e.g., double layers / localized acceleration structures) that appear as preferred modes of R^*.

5.2 Interpretive map

- Generator region → imposed driving boundary condition (effective EMF in starred form).
- Transmission region → Alfvénic channel with ledger-native line parameters $(Z_{\mathrm{APM}}, Y_{\mathrm{APM}})$.
- Load region → closure operator producing R^* (possibly multi-modal), consistent with long-standing current–voltage viewpoints in auroral acceleration [Knight, 1973, Morooka et al., 2004].

6 Falsifiable Gates (A1–A3)

6.1 Gate A1: Resistance clustering

Statement. Over ensembles of auroral/FAC events, R^* exhibits stable clustering into preferred values after normalization by geometry (and event classification), rather than filling a continuum.

APM rationale (ledger quantization). In the APM, the FAC channel is treated as a ledger-closure conduit rather than a purely constitutive medium. The working hypothesis is that closure across generator–transmission–load admits a *discrete mode index* $N \in \mathbb{N}$ (counting admissible "closure quanta" of Aether rotation/torsion in the channel), so that the effective acceleration operator selects from a discrete family

$$R^* \in \{R^*_N\}_{N\in\mathbb{N}},$$

up to smooth geometric normalization. In this view, observed clustering is the operational signature of the quantum (discrete) nature of ledger balance, not an artifact of binning.

Operational test.

1. Estimate $\mathcal{I}^*$ from FAC products (magnetometer-derived $J_\parallel$ integrated over an inferred tube area, or directly from integrated current estimates).
2. Estimate Φ^* from measured/inferred $E_\parallel$ structures or from particle energy spectra as a proxy for potential drop [Mozer and Hull, 2001, Carlson et al., 1998, Ergun et al., 2004].
3. Form $R^* = \Phi^*/\mathcal{I}^*$ and test for persistent multimodality (cluster stability under sensible geometry normalizations).

Failure condition. No stable clustering is observed under repeated normalization choices; R^* behaves as an unconstrained nuisance parameter.

6.2 Gate A2: Monotone closure under driving

Statement. Within a regime, $(\Phi^*, \mathcal{I}^*)$ follows an approximately single-valued "load curve"; regime transitions correspond to the onset of localized boundary operators (strong acceleration structures).

Operational test. Condition on a driving proxy (choose one and keep it fixed across the study) and evaluate whether $\Phi^*(\mathcal{I}^*)$ is reproducible in that regime, in the same spirit as established auroral current–voltage analyses [Knight, 1973, Morooka et al., 2004].

Failure condition. No reproducible $\Phi^*(\mathcal{I}^*)$ relation emerges even after regime conditioning.

6.3 Gate A3: Saturation as a ledger cap

Statement. There exists a geometry-dependent cap

$$\mathcal{I}^* \le \mathcal{I}^*_{\max}(\text{geometry}), \tag{15}$$

such that increased driving leads primarily to restructuring (new channels, filament splitting, new boundary operators) rather than unbounded growth in $\mathcal{I}^*$.

APM rationale (ledger capacity and topological breakdown). In APM/QMU, a field-aligned current channel is modeled as a torsional throughput conduit in which the local ledger density (in curl per available cross-section) cannot increase without limit. The hypothesis behind Eq. (15) is that the Aether unit admits a *maximum admissible torsion/curvature density* before topological breakdown occurs: beyond this capacity, the geometry cannot sustain additional current in the same channel, and the closure must reorganize into a new topology (e.g., filamentation, channel splitting, or the formation of additional boundary operators such as double layers). This is the ledger analogue of a wire "fusing current": the system preserves global closure by changing the channel topology rather than permitting an unbounded increase in $\mathcal{I}^*$ within a fixed geometry.

Operational test. Use global FAC reconstructions or repeated passes to test whether $\mathcal{I}^*$ saturates while other observables (e.g., event complexity, multiplicity of channels) increase. Storm-time global FAC studies provide concrete observational contexts in which saturation-like behavior has been evaluated using Iridium/AMPERE-era reconstructions [Anderson et al., 2000, Anderson and Korth, 2007].

Failure condition. $\mathcal{I}^*$ scales without cap under strong driving after controlling for geometry.

7 Data Products and Inference in Starred Variables

7.1 What must be inferred (minimal closure tuple)

For each event (spacecraft crossing or reconstructed interval), the minimal closure tuple is

$$(\mathcal{I}^*, \Phi^*, R^*), \qquad R^* = \Phi^*/\mathcal{I}^*,$$

with optional geometric companions such as a normalized tube cross-section $A^* := A/{\lambda_C}^2$ and a normalized path length $L^* := L/\lambda_C$ for inter-event comparability.

7.2 FAC inference pathway (magnetometer-derived products)

Most observational pipelines provide either a field-aligned current density estimate $J_\parallel$ along the spacecraft track, or an integrated current estimate I for a mapped current sheet/flux tube. Global reconstructions based on Iridium engineering magnetometers and derived products (including AMPERE-era workflows) provide a practical path for large-ensemble testing [Anderson et al., 2000, Waters et al., 2001, Coxon et al., 2018].

Pathway 1: integrated current available. If an event analysis provides an integrated current I (through a specified cross-section), then the QMU-normalized current is defined directly by

$$\mathcal{I}^* := \frac{I}{{e_{\max}}^2 F_q}. \tag{16}$$

Pathway 2: current density available. If the product provides $J_\parallel$, infer a tube (or sheet) cross-section A via a chosen mapping model and define

$$I := \int_A J_\parallel \, \mathrm{d}A, \qquad \mathcal{I}^* := \frac{1}{{e_{\max}}^2 F_q} \int_A J_\parallel \, \mathrm{d}A. \tag{17}$$

To keep everything ledger-native, it is helpful to also record the normalized area

$$A^* := \frac{A}{{\lambda_C}^2}. \tag{18}$$

and (if needed) the normalized current density

$$\mathcal{J}_\parallel^* := \frac{J_\parallel}{{e_{\mathrm{emax}}}^2\, {F_q}/{\lambda_C}^2}, \qquad \mathcal{I}^* = \int_{A^*} \mathcal{J}_\parallel^*\, \mathrm{d}A^*. \tag{19}$$

7.3 Parallel potential drop inference pathway

There are two complementary approaches. The template assumes you will declare which proxy chain you used for each event.

Pathway 1: field integration (direct, when $E_\parallel$ is available). Given a reconstructed field-aligned profile $E_\parallel(\ell)$ along a path segment of length L, define

$$\mathcal{E}_\parallel^* := \frac{E_\parallel}{m_\mathrm{e}\, {F_q}^2 \lambda_C / {e_{\mathrm{emax}}}^2}, \qquad \ell^* := \frac{\ell}{\lambda_C}, \qquad \Phi^* := \int_0^{L^*} \mathcal{E}_\parallel^*(\ell^*)\, \mathrm{d}\ell^*, \tag{20}$$

where $L^* := L/\lambda_C$. Canonical observational contexts include quasi-static parallel fields and acceleration regions inferred from combined fields/particles [Mozer and Hull, 2001, Carlson et al., 1998, Ergun et al., 2004].

Pathway 2: particle-spectrum proxy (indirect, robust for large ensembles). When a clear acceleration signature exists in the particle energy spectrum (e.g., a characteristic cutoff, peak, or plateau feature), define a dimensionless energy marker

$$\varepsilon^* := \frac{\varepsilon}{m_\mathrm{e} {F_q}^2 {\lambda_C}^2}, \tag{21}$$

and use a declared proxy map

$$\Phi^* \approx \mathcal{K}\, \varepsilon^*, \tag{22}$$

where the dimensionless factor $\mathcal{K}$ encodes the chosen interpretation (monoenergetic drop, partial filling, pitch-angle selection, multi-step acceleration, etc.). In APM terms, $\mathcal{K}$ is part of the *operator choice* for the acceleration boundary, and it should be held fixed within a regime classification when testing Gates A1–A3.

7.4 Effective resistance and power in starred form

Once $\mathcal{I}^*$ and Φ^* are formed, define

$$R^* := \frac{\Phi^*}{\mathcal{I}^*}. \tag{23}$$

It is also useful to track a dimensionless power throughput (per event or per unit normalized length/area, depending on the chosen reduction). A minimal event-level measure is

$$\mathcal{P}_{\mathrm{evt}}^* := \mathcal{I}^*\, \Phi^*. \tag{24}$$

7.5 Geometry normalization (what must be recorded)

To distinguish "physics" from mapping artifacts, each event record should include:

- a geometry label (e.g., oval sector / latitude bin / local time bin / region-1 vs region-2 classification),
- the normalized length scale $L^* := L/\lambda_C$ used for the Φ^* estimate,
- the normalized area scale $A^* := A/{\lambda_C}^2$ used for the $\mathcal{I}^*$ estimate (when applicable),
- a regime tag identifying the inference chain: field-integration vs particle-proxy, and the chosen $\mathcal{K}$ if the particle proxy is used.

7.6 Practical note on "ledger proxies"

In observational practice, A_u and curl are not measured as primitive laboratory standards in situ; rather, they enter through ledger normalization (e.g., $c = F_q\lambda_C$ and Ledger One). This is intentional: Gates A1–A3 are designed to be evaluated on derived starred variables, with the ledger serving as the closure constraint.

7.7 Toy numerical illustration (resn-normalized) and actionable gate checks

To make Gates A1–A3 directly actionable, we include a toy illustration in which the starred variables

$$\mathcal{I}^* = \frac{\dot{Q}}{{e_{\mathrm{emax}}}^2\, F_q}, \qquad \Phi^* = \int \mathcal{E}^*_{\parallel}\, \mathrm{d}\ell^*, \qquad R^* = \frac{\Phi^*}{\mathcal{I}^*},$$

are computed and interpreted *explicitly in QMU units*, where R^* is "resistance in resn units" by construction (see Eqs. (6) and (13)). This illustration is motivated by canonical auroral acceleration observations in which quasi-static parallel potential structures and double layers support current closure [Ergun et al., 2004, Mozer and Hull, 2001, Carlson et al., 1998].

Important note (QMU-only illustration). The numerical values below are illustrative and are presented entirely in starred variables (no SI). A reader wishing to reproduce $\mathcal{I}^*$ and Φ^* from any specific event in the cited literature should use the proxy chains in Section 7.7 together with the charge convention in Eq. (4), expressing any plasma-derived e^2 factors in the QMU base charge ${e_{\mathrm{emax}}}^2$.

Toy A1 illustration: hypothetical clustering of R^* in resn units

Consider six events in a single regime classification (same geometry bin, same proxy choice $\mathcal{K}$). Compute $(\mathcal{I}^*, \Phi^*, R^*)$ for each event:

Table 1: Toy example: computing $(\mathcal{I}^*, \Phi^*, R^*)$ and exhibiting hypothetical clustering of R^* (resn-normalized).

Event	$\mathcal{I}^*$	Φ^*	$R^* = \Phi^*/\mathcal{I}^*$
1	1.00	0.50	0.50
2	0.96	0.49	0.51
3	1.04	0.52	0.50
4	1.00	2.00	2.00
5	1.03	2.06	2.00
6	0.97	1.94	2.00

In Gate A1, one would histogram R^* over a large ensemble (after geometry normalization) and test whether peaks persist (here near $R^* \approx 0.5$ and $R^* \approx 2.0$) rather than filling a continuum. In the APM interpretation, these peaks represent discrete closure modes of the acceleration boundary operator.

Toy A3 illustration: saturation of $\mathcal{I}^*$ with restructuring

For Gate A3, introduce an event-level driving proxy D^* (dimensionless; chosen and held fixed across a study) and a simple restructuring marker M (e.g., number of distinct current channels or acceleration structures identified in the interval). A toy saturation pattern is:

Table 2: Toy example: saturation as a ledger cap. As driving increases, $\mathcal{I}^*$ approaches a cap while the system restructures (increasing M) and/or increases Φ^*.

Case	D^*	$\mathcal{I}^*$	$(\Phi^*,\ M)$
A	1	10	(0.6, 1)
B	2	20	(1.2, 1)
C	3	35	(1.9, 1)
D	4	50	(2.6, 2)
E	5	50	(3.4, 3)

Gate A3 is satisfied if, after controlling for geometry, $\mathcal{I}^*$ exhibits a stable cap $\mathcal{I}^*_{\max}$ while increasing driving is expressed primarily through restructuring (increasing M) and/or through changes in Φ^* rather than through unbounded growth in $\mathcal{I}^*$.

How to operationalize on real datasets.

- Choose a regime classification and geometry normalization (oval sector, local time, region-1/region-2, etc.) [Iijima and Potemra, 1978, Coxon et al., 2018].
- Choose a proxy chain for Φ^* (field-integration or particle proxy) and hold its parameters fixed within the regime (e.g., fixed $\mathcal{K}$).
- Compute $\mathcal{I}^*$ using ${e_{\text{emax}}}^2$ as the base charge; apply Eq. (4) when plasma formulations introduce e^2.
- Test A1 by stability of R^* clusters; test A3 by stability of $\mathcal{I}^*_{\max}$ and co-variation with a restructuring marker M.

8 APM Predictions Beyond the Gates (Optional Extensions)

8.1 Channel "impedance" selection

Discuss how Z_{APM} may function as a baseline stiffness scale and how departures correspond to non-ideal closure (boundary operators).

8.2 Multi-channel closure

Introduce a parallel/series effective model in starred variables:

$$R^{*-1}_{\mathrm{eff}} = \sum_k (R^*_k)^{-1} \quad \text{(parallel channels)}, \qquad R^*_{\mathrm{eff}} = \sum_k R^*_k \quad \text{(series segments)}.$$

Emphasize that these are bookkeeping identities for closure modes.

9 Proposed Experiments and Observation Campaigns

9.1 Archive-only retrospective test (no new hardware)

Describe a minimal study: select events, compute $(\mathcal{I}^*, \Phi^*, R^*)$, test A1–A3. Note that global reconstructions enable large ensembles without new instrumentation [Anderson et al., 2000, Waters et al., 2001, Coxon et al., 2018].

9.2 Targeted conjunction test

Propose a conjunction between: (i) low-altitude FAC mapping, (ii) in situ fields/particles in the acceleration region, (iii) ground conductance proxies. State what must be measured to close R^*.

9.3 Laboratory analog (optional)

If desired, propose a scaled plasma column or double-layer experiment where the same starred observables can be formed and compared to auroral clustering, using the charge conversion Eq. (4) to keep the reduction ledger-native.

10 Discussion

10.1 Interpretation of outcomes

- If A1 holds: boundary operators correspond to discrete ledger-closure modes.
- If A2 holds: load curves exist; regime changes are closure bifurcations.

- If A3 holds: saturation is a geometry/ledger constraint, not a parameter accident (compare observational saturation analyses of global FACs and related coupling limits) [Anderson and Korth, 2007, Siscoe et al., 2002, Hairston et al., 2003].

10.2 Relation to other APM work

Connect to ledger closure philosophy and to any existing QADI operator/closure tests already in your series.

11 Conclusion

Summarize the framework, the three observables, and the three gates.

A Algebraic identities from Ledger One

From Eq. (3):

$$A_u \,\mathrm{curl} = c^2 \quad \Rightarrow \quad \frac{A_u}{\mathrm{curl}} = \frac{c^2}{\mathrm{curl}^2} \quad \Rightarrow \quad \sqrt{\frac{A_u}{\mathrm{curl}}} = \frac{c}{|\mathrm{curl}|}.$$

State the convention under which $|\mathrm{curl}| = \mathrm{curl}$.

B Notes on sign/orientation conventions

If curl is used as an oriented quantity, specify the signed convention and keep Z_{APM} as a magnitude.

Acknowledgments

The Quantum AetherDynamics Institute (QADI) is a private 501(c)(3) research institute developing the Aether Physics Model (APM) and Quantum Measurement Units (QMU). Thomson III [2025] Publications and data are archived with DOIs in the AetherPhysics Zenodo community: zenodo.org/communities/aetherphysics.

References

Hannes Alfvén. *Cosmic Plasma*, volume 82 of *Astrophysics and Space Science Library*. Springer, 1981. ISBN 9027711518. URL https://link.springer.com/book/10.1007/978-94-009-8374-8.

B. J. Anderson and H. Korth. Saturation of global field aligned currents observed during storms by the Iridium satellite constellation. *Journal of Atmospheric and Solar-Terrestrial Physics*, 69(1–2):166–169, 2007. doi: 10.1016/j.jastp.2006.06.013. URL https://doi.org/10.1016/j.jastp.2006.06.013.

B. J. Anderson, K. Takahashi, and B. A. Toth. Sensing global Birkeland currents with Iridium® engineering magnetometer data. *Geophysical Research Letters*, 27(24):4045–4048, 2000. doi: 10.1029/2000GL000094. URL https://doi.org/10.1029/2000GL000094.

C. W. Carlson, J. P. McFadden, R. E. Ergun, M. Temerin, W. Peria, F. S. Mozer, D. M. Klumpar, E. G. Shelley, W. K. Peterson, E. Möbius, R. Elphic, R. Strangeway, C. A. Cattell, and R. Pfaff. Fast observations in the downward auroral current region: Energetic upgoing electron beams, parallel potential drops, and ion heating. *Geophysical Research Letters*, 25(12):2017–2020, 1998. doi: 10.1029/98GL00851. URL https://doi.org/10.1029/98GL00851.

J. C. Coxon, S. E. Milan, and B. J. Anderson. A review of Birkeland current research using AMPERE, 2018. URL https://doi.org/10.1002/9781119324522.ch16.

R. E. Ergun, Y.-J. Su, L. Andersson, C. W. Carlson, J. P. McFadden, F. S. Mozer, D. L. Newman, M. V. Goldman, and R. J. Strangeway. Auroral particle acceleration by strong double layers: The upward current region. *Journal of Geophysical Research: Space Physics*, 109(A12):A12220, 2004. doi: 10.1029/2004JA010545. URL https://doi.org/10.1029/2004JA010545.

M. R. Hairston, T. W. Hill, and R. A. Heelis. Observed saturation of the ionospheric polar cap potential during the 31 march 2001 storm. *Geophysical Research Letters*, 30(6):1325, 2003. doi: 10.1029/2002GL015894. URL https://doi.org/10.1029/2002GL015894.

T. Iijima and T. A. Potemra. The amplitude distribution of field-aligned currents at northern high latitudes observed by Triad. *Journal of Geophysical Research*, 81(13):2165–2174, 1976. doi: 10.1029/JA081i013p02165. URL https://doi.org/10.1029/JA081i013p02165.

T. Iijima and T. A. Potemra. Large-scale characteristics of field-aligned currents associated with substorms. *Journal of Geophysical Research*, 83(A2):599–615, 1978. doi: 10.1029/JA083iA02p00599. URL https://doi.org/10.1029/JA083iA02p00599.

S. Knight. Parallel electric fields. *Planetary and Space Science*, 21(5):741–750, 1973. doi: 10.1016/0032-0633(73)90093-7. URL https://doi.org/10.1016/0032-0633(73)90093-7.

M. W. Morooka, T. Mukai, and H. Fukunishi. Current-voltage relationship in the auroral particle acceleration region. *Annales Geophysicae*, 22:3641–3653, 2004. doi: 10.5194/angeo-22-3641-2004. URL https://doi.org/10.5194/angeo-22-3641-2004.

F. S. Mozer and A. Hull. Origin and geometry of upward parallel electric fields in the auroral acceleration region. *Journal of Geophysical Research: Space Physics*, 106(A4):5763–5778, 2001. doi: 10.1029/2000JA900117. URL https://doi.org/10.1029/2000JA900117.

G. L. Siscoe, N. U. Crooker, and K. D. Siebert. Transpolar potential saturation: Roles of region 1 current system and solar wind ram pressure. *Journal of Geophysical Research: Space Physics*, 107 (A10):1321, 2002. doi: 10.1029/2001JA009176. URL https://doi.org/10.1029/2001JA009176.

David W. Thomson III. Quantum aetherdynamics institute (qadi): Community doi overview and citation guide. Zenodo, 2025. URL https://doi.org/10.5281/zenodo.17479314.

C. L. Waters, B. J. Anderson, and K. Liou. Estimation of global field aligned currents using the Iridium® system magnetometer data. *Geophysical Research Letters*, 28(11):2165–2168, 2001. doi: 10.1029/2000GL012725. URL https://doi.org/10.1029/2000GL012725.